




Contrast-enhanced MRI could predict response of systemic therapy in advanced intrahepatic cholangiocarcinoma

Ruofan Sheng^{1,2} · Xiaoyong Huang⁴ · Kaipu Jin^{1,3} · Shanshan Gao^{1,3} · Mengsu Zeng^{1,3}  · Dong Wu^{1,3} · Guoming Shi⁴

Received: 4 November 2021 / Revised: 11 January 2022 / Accepted: 17 February 2022 / Published online: 17 March 2022

© The Author(s), under exclusive licence to European Society of Radiology 2022

Abstract

Objective To investigate whether pre-treatment contrast-enhanced MRI could predict the therapeutic response of systemic treatment in advanced intrahepatic cholangiocarcinoma (ICC).

Methods This retrospective study enrolled 61 ICC participants with contrast-enhanced MRI before combined systemic therapy. Clinical characteristics and MRI features were compared between patients with and without therapeutic response by univariate and multivariate logistic regression analyses. Then, a combined MRI-based model and the nomogram were established based on the results of the multivariate analysis. The diagnostic performances of significant findings and the combined model were evaluated and compared. The progression-free survival (PFS) rates between patients with high and low combined index values were compared.

Results Thirty (49.18%) patients showed overall response after therapy. In multivariate analysis, tumor margin (odds ratio (OR) = 5.004, $p = 0.014$), T2 homogeneity (OR = 14.93, $p = 0.019$), and arterial peritumoral enhancement (OR = 5.076, $p = 0.042$) were independent predictive factors associated with therapeutic response. The C-index with the formulated nomogram incorporating the three independent imaging features was 0.828 (95% CI 0.710–0.913). Diagnostic characteristics of the combined index were superior to any single feature alone ($p = 0.0007$ – 0.0141). ICCs with high combined index values showed higher PFS rates than those with low values ($\chi^2 = 13.306$, $p < 0.0001$).

Conclusions Pre-treatment contrast-enhanced MRI can be used to predict therapeutic response in advanced ICC with systemic therapy. The combination model incorporating significant MRI features achieved an improved predictive value, which may play an important role in identifying appropriate therapeutic candidates.

Key Points

- Contrast-enhanced MRI can predict response of systemic therapy in advanced ICC.
- MRI features of tumor margin, T2 homogeneity, and arterial peritumoral enhancement are related to therapeutic response.
- The combined MRI-based model may help to identify appropriate therapeutic candidates.

Keywords Magnetic resonance imaging · Cholangiocarcinoma · Combination treatment

Mengsu Zeng and Dong Wu contribute the same as corresponding authors.

✉ Mengsu Zeng
mengsuzeng@163.com

✉ Dong Wu
wu_dong2021@163.com

² Zhongshan Xiamen Hospital, Fudan University, Shanghai, China

³ Shanghai Institute of Medical Imaging, Shanghai, China

⁴ Department of Liver Surgery, Zhongshan Hospital, Fudan University, Shanghai, China

¹ Department of Radiology, Zhongshan Hospital, Fudan University, No. 180 Fenglin Road, Xuhui District, Shanghai 200032, China

Abbreviations

ADC	Apparent diffusion coefficient
APE	Arterial peritumoral enhancement
AUC	Area under the curve
CI	Confidence interval
ICC	Intrahepatic cholangiocarcinoma
MRI	Magnetic resonance imaging
OR	Odds ratio
PD-1	Programmed cell death protein 1
PFS	Progression-free survival
RECIST	Response Evaluation Criteria in Solid Tumors
ROI	Region of interest

Introduction

Intrahepatic cholangiocarcinoma (ICC) is the second most common primary liver cancer after hepatocellular carcinoma, it is a highly lethal hepatobiliary malignancy with poor prognosis, and most patients are at advanced stages that preclude surgical resection once confirmed [1, 2]. For these patients, systemic therapies including cytotoxic chemotherapy, targeted therapy, and immunotherapy have shown effectiveness. Gemcitabine plus platinum-based antitumor drugs has been a standard of care for first-line regimen in advanced ICC, and the Gemox regimen (oxaliplatin+gemcitabine) is a frequently preferred well-established regimen nowadays [3, 4], but the efficacy is still not satisfactory. Multiple tyrosine kinase inhibitors including sorafenib and lenvatinib with anti-angiogenic effects have been proven effective in hepatocellular carcinoma [5, 6], and their antitumor activity has also been demonstrated in biliary tract cancers [7]. In recent years, immunotherapies with checkpoint blockade inhibitors including the anti-programmed cell death protein 1 (PD-1) antibody have shown remarkable therapeutic values in the treatment of hepatobiliary tumors [8–10]. Combined with other means such as chemotherapy and targeted drugs is an important direction to improve the therapeutic effect of immunological checkpoint inhibitors [2].

However, differential responses to the combined systemic therapy have been observed with frequent primary or secondary resistance. Moreover, due to the high cost and inevitable adverse effects, a reliable biomarker, especially the non-invasive approach, to predict response to the systemic treatment is urgently needed to search for appropriate therapeutic candidates and optimize individual treatment strategies. Among imaging techniques, magnetic resonance imaging (MRI) is superior to other liver imaging modalities including ultrasonography and computed tomography as it provides multiparametric information with no radiation exposure [11, 12]. Nowadays, MRI has been increasingly performed in routine clinical care for liver cancer patients, making the imaging assessment a practical and cost-effective non-invasive evaluation tool. Recent studies have demonstrated the potential of

MRI in prognostic evaluations of ICC [13–15], but barely involved the efficacy evaluation with combined systemic therapy.

In this study, we aimed to investigate whether pre-treatment MRI could predict the therapeutic response of systemic treatment in advanced ICC.

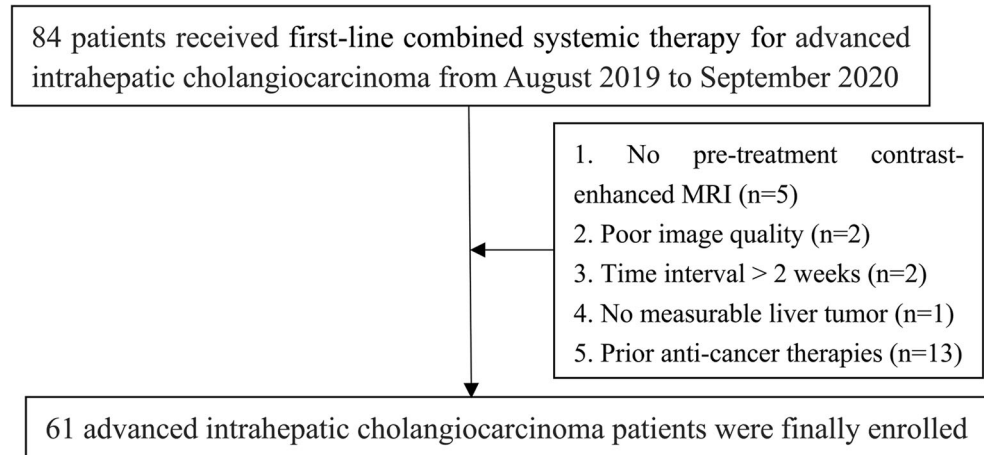
Materials and methods

Patients

The institutional review board approved this retrospective study and waived the requirement for informed consent regarding the acquisition of MR imaging data. The study was conducted in advanced ICC patients who received first-line combined systemic therapy from two prospective clinical trials with anti-angiogenic agent Lenvatinib (registered with [ClinicalTrials.gov](https://clinicaltrials.gov) (NCT04361331) with PD1 antibody + Lenvatinib (group 1) or Gemox chemotherapy + Lenvatinib (group 2), and (NCT03951597) with combined Gemox chemotherapy, Lenvatinib, and PD-1 antibody (group 3)) from August 2019 to September 2020. All patients were pathologically confirmed by liver biopsy before treatment. Exclusion criteria of the present study were (1) no availability of pre-treatment contrast-enhanced MRI in our institution; (2) poor image quality due to severe artifacts; (3) time interval between MR scan and therapy more than 2 weeks; (4) no measurable tumor in the liver according to the guideline of Response Evaluation Criteria in Solid Tumors version 1.1 (RECIST v1.1); and (5) history of prior local-regional or systemic anti-cancer therapies (Fig. 1).

Image acquisition

All patients were examined before therapy with a 3.0-T MR scanner (uMR 770; United Imaging Healthcare) with body phased-array coils. Routine plain-scan liver protocols consisted of axial respiratory-triggered T2-weighted fat-suppressed fast spin-echo sequence, T1-weighted in-phase and opposed-phase gradient-echo sequence, and free-breathing single-shot spin-echo echo-planar diffusion-weighted sequence (b values, 0, 50, and 500 s/mm²) with automatically generated apparent diffusion coefficient (ADC) maps. Dynamic imaging was performed with axial breath-hold T1-weighted 3-dimensional fat-suppressed gradient-echo sequence, before and after the intravenous administration of gadopentetate dimeglumine (Magnevist; Bayer HealthCare). Contrast was administered at a dose of 0.1 mmol/kg at a rate of 2 mL/s, followed by a 20-mL saline flush using a power injector (Spectris; Medrad). The arterial phase acquisitions were triggered automatically when contrast media reached the ascending aorta; the portal venous and delay phase were

Fig. 1 Flowchart of patient selection

performed at 60 s and 180 s, respectively. Detailed scanning parameters of each sequence are listed in Table 1.

Image analysis

MR images were independently evaluated by two radiologists (with 6 and 10 years of experience in abdominal imaging, respectively) using a picture archiving and communication system (Pacspeed, GE Medical Systems Integrated Imaging Solutions, Prospect). The reviewers were aware that the patients had systemic treatment for ICC, but were unaware of other information, including patients' history, laboratory results, and follow-up information. The MR images were randomly presented to avoid bias by creating a clinical practice setting. In cases with multiple lesions in the liver, only the major target lesion was analyzed.

Qualitative analysis

The following MRI features were evaluated: (a) location (right/left/right and left/caudate lobe); (b) tumor margin (smooth: sharp, well-defined tumor with smooth contour/

irregular: indistinct, ill-defined tumor with irregular contour), tumor margin was evaluated on T2-weighted images; (c) signal homogeneity on T2WI (homogeneous: the entire tumor was uniform as a whole with homogeneous signal inside/heterogeneous: the entire tumor was nonuniform as a whole with relatively hyper- or hypointense portion compared with the main body of tumor), a cutoff of 10% heterogeneous regions on T2WI was regarded as a positive finding ($\geq 10\%$ of the entire tumor), and heterogeneous regions less than 10% were defined as homogeneous; (d) arterial enhancement pattern (non-rim enhancement/rim enhancement/no enhancement); (e) enhancement intensity on arterial phase (marked: approximately equal to aorta/moderate: approximately equal to portal vein/mild: less than portal vein); (f) enhancement pattern (progressive: the range or intensity of enhancement progressed over time/persistent: the enhancement remained invariable through all phases/degressive: decreasing enhancement over time); (g) arterial peritumoral enhancement (APE): fuzzy-margined hyperenhancement outside the tumor borders that becomes isointense with normal liver parenchyma in later dynamic phases; (h) signal in diffusion-weighted imaging

Table 1 Sequence parameters

Parameter	T1-weighted IP and OP imaging	Contrast-enhanced T1-weighted imaging	T2-weighted imaging	Diffusion-weighted imaging
Repetition time (ms)	3.66	3.27	2000	2714
Echo time (ms)	1.2/2.4	1.45	106.2	63.3
Field of view (mm ²)	400 × 300	400 × 300	380 × 380	380 × 300
Matrix	168 × 288	288 × 320	256 × 256	128 × 100
Section thickness (mm)	3	3	6	6
Gap (mm)	0	0	1.2	1.2
Flip angle (degree)	10	10	100	90

IP in-phase, OP opposed-phase

with b value of 500 s/mm^2 (non-rim hyper-/rim hyper-/isohypointensity); (i) targetoid appearance (rim arterial phase hyperenhancement, peripheral washout, delayed central enhancement, or targetoid restriction on diffusion-weighted imaging); (j) hemorrhage; (k) necrosis; (l) hepatic capsule retraction; (m) intrahepatic bile duct dilation. After the first independent image analyses by the two radiologists, interobserver agreements were assessed. In discordant cases, a consensus was made for final decision.

Quantitative analysis

For the measurement of ADC values, regions of interest (ROIs) were manually drawn on the diffusion-weighted images, including the solid tumor area as large as possible; these ROIs were then copied onto the ADC maps; and the ADC values were assessed. For each case, 3 ROIs were placed on 3 subsequent slice locations and the average value was used. Great care was taken to avoid large vessels, necrosis, hemorrhage, and artifacts. Mean values measured by two observers were then averaged for final analyses. Lesion size was measured at the largest cross-sectional diameter (the maximum dimension) on the axial planes of the delay phase.

Follow-up and treatment assessment

All patients were treated and monitored regularly. Treatment was continued until the tumor progressed or unacceptable toxicity developed. Tumor response was evaluated via contrast-enhanced MRI/CT every 2 months (± 2 weeks) during therapy. Response of patients was determined according to RECIST v1.1 [16], and then divided into the response group: patients with a best overall response of complete response or partial response, and non-response group: patients with a best overall response of stable disease or progression disease. The additional endpoint of this study was progression-free survival (PFS), which was determined from the initiation of treatment to the date of progression disease or death, whichever occurred first. The cutoff follow-up date for this research was September 30, 2021.

Statistical analysis

Statistical analyses were conducted using the SPSS software (version 22.0) and R software (version 3.4.1). All tests were two-sided, and $p < 0.05$ was considered significant. The normality of the data was tested using the Kolmogorov-Smirnov test, and the homogeneity of variances was tested using Levene's method. Interobserver agreement was calculated by using interclass correlation coefficient: poor for less than 0.20, fair for 0.20–0.40, moderate for 0.40–0.60, good for 0.60–0.80, and excellent for 0.80–1.00. The clinical and imaging findings were compared between patients with and

without response. Continuous variables were compared using the independent t -test or Mann-Whitney U test, and categorical variables were compared using Pearson's χ^2 test or Fisher's exact test, as appropriate. Factors with a p -value less than 0.05 in univariate analyses were entered into the multivariate models. Multivariate logistic regression analysis was performed using the backward stepwise elimination method to identify the independent predictors. The Hosmer-Lemeshow test was performed to explain the goodness-of-fit for the multivariate logistic model. A nomogram was established based on the results of the multivariable analysis. Receiver operating characteristic curve analyses of significant findings and the combined index were performed to evaluate the diagnostic performances. Sensitivity, specificity, positive likelihood ratio, and negative likelihood ratio with 95% confidence interval (CI) were calculated. The areas under the curve (AUCs) were compared using DeLong's method. In addition, the threshold value of the combined index was evaluated based on the best Youden's index on the receiving operating characteristic curve, and the combined index was divided into the high-value group and low-value group accordingly. PFS was estimated using the Kaplan-Meier method, and PFS rates between patients with high and low values of the combined index as well as patients among the three different therapeutic groups were compared by the log-rank test. In addition, a Cox regression model was constructed to examine if the combined index had significant predictive ability for PFS when adjusting with the possible confounding factor of different therapeutic groups.

Results

Patients

A total of 61 patients were enrolled in our research, including 36 men and 25 women with a mean age of 57.67 ± 10.31 years (range, 33–75 years). The median follow-up period was 16 months (range, 2–20 months). Patients' distributions of the 3 therapeutic groups were as follows: group 1 ($n = 21$), group 2 ($n = 18$), and group 3 ($n = 22$). Among all, complete response, partial response, stable disease, and progression disease were achieved in 0 (0%), 30 (49.18%), 25 (40.98%), and 6 (9.84%) patients, respectively. Finally, 30 (49.18%) patients showed overall response, and 31 (50.82%) patients showed no response. The baseline characteristics of patients are shown in Table 2. There were no differences in patients' age, sex, tumor markers, or any clinical characteristics between the response and non-response groups ($p = 0.053$ – 1.000). Therapeutic regimens were not equally distributed over different response groups, but no significant differences existed as a whole ($\chi^2 = 5.323$, $p = 0.070$), while pairwise comparisons showed a different distribution between therapeutic groups 2 and 3 (χ^2

Table 2 Clinical characteristics of intrahepatic cholangiocarcinoma according to therapeutic response

Variables	Response (<i>n</i> = 30)	No response (<i>n</i> = 31)	<i>p</i>
Age (y)†	58.87 ± 11.66	56.52 ± 8.85	0.378
Sex male/female	17 (56.7)/13 (43.3)	19 (61.3)/12 (38.7)	0.797
Vascular invasion Y/N	24 (80.0)/6 (20.0)	30 (96.7)/1 (3.3)	0.053
Lymphatic metastasis Y/N	18 (60.0)/12 (40.0)	23 (74.2)/8 (25.8)	0.283
Distant metastasis Y/N	8 (26.7)/22 (73.3)	9 (29.0)/22 (71.0)	1.000
Hepatitis B virus Y/N	11 (36.7)/19 (63.3)	9 (29.0)/22 (71.0)	0.592
Alpha fetoprotein <20/> 20 ng/mL	26 (86.7)/4 (13.3)	22 (71.0)/9 (29.0)	0.211
Carcinoembryonic antigen <5/> 5 ng/mL	25 (83.3)/5 (16.7)	22 (71.0)/9 (29.0)	0.363
Carbohydrate antigen 199 <37/> 37 ng/mL	12 (40.0)/18 (60.0)	10 (32.3)/21 (67.7)	0.600
Total bilirubin <20.4/> 20.4 μmol/L	26 (86.7)/4 (13.3)	30 (96.7)/1 (3.3)	0.195
Direct bilirubin <6.8/> 6.8 μmol/L	26 (86.7)/4 (13.3)	27 (87.1)/4 (12.9)	1.000
Alanine aminotransferase <40/> 40 U/L	25 (83.3)/5 (16.7)	28 (90.3)/3 (9.7)	0.237
Aspartate aminotransferase <35/> 35 U/L	24 (80.0)/6 (20.0)	25 (80.6)/6 (19.4)	1.000
Platelet count <100/> 100 × 10 ⁹ /L	1 (3.3)/29 (96.7)	3 (9.7)/28 (90.3)	0.612
Prothrombin time <13.0/> 13.0 s	27 (90.0)/3 (10.0)	30 (96.7)/1 (3.3)	0.354
Therapeutic groups 1/2/3	9 (30.0)/6 (20.0)/15 (50.0)	12 (38.7)/12 (38.7)/7 (22.6)	0.070

Unless otherwise specified, data are numbers of patients, with percentage in parentheses

† Data are mean ± standard deviation

Qualitative variables are analyzed using Pearson's χ^2 test or Fisher's exact test as appropriate, and quantitative variables are analyzed using the independent *t*-test

= 4.821, $p = 0.028$), but not between groups 1 and 2 ($\chi^2 = 0.371$, $p = 0.542$) and between groups 1 and 3 ($\chi^2 = 2.794$, $p = 0.095$).

MR imaging characteristics of ICC related to therapeutic response

As presented in Table 3, imaging characteristics of tumor number ($\chi^2 = 11.726$, $p = 0.003$), tumor margin ($\chi^2 = 8.795$, $p = 0.005$), T2 homogeneity ($\chi^2 = 10.789$, $p = 0.001$), and APE ($\chi^2 = 8.925$, $p = 0.003$) were associated with therapeutic response (Figs. 2 and 3). Interobserver agreements were good to excellent for all qualitative imaging parameters (interclass correlation coefficient = 0.702–0.965). Mean tumor size of the cases with no response was larger than that with response (mean 7.542 ± 2.824 cm vs 6.527 ± 2.202 cm), but no statistical differences existed ($t = 1.562$, $p = 0.124$). Although average ADC values in the non-response group were lower than those in the response group (median 1.107 (interquartile ranges 0.908–1.409) × 10³ mm²/s vs 1.283 (1.083–1.468) × 10³ mm²/s), the differences were also not significant ($p = 0.162$) and interobserver agreement was excellent

for ADC measurement (interclass correlation coefficient = 0.985 (95% CI 0.975–0.991)).

In multivariate analysis, smooth margin (odds ratio (OR) = 5.004 (95% CI: 1.384, 18.095), $p = 0.014$), homogeneous T2 signal (OR = 14.93 (95% CI: 1.550, 142.86), $p = 0.019$), and non-APE (OR = 5.076 (95% CI: 1.057, 24.39), $p = 0.042$) were independent predictive factors associated with therapeutic response. The Hosmer-Lemeshow test significance level was 0.893, suggesting an acceptable goodness-of-fit for the model. To create a more accurate and useful predictive model, we tried to integrate all the significant radiological variables, and a regression coefficient-based nomogram was constructed (Fig. 4). In our cohort, the C-index for therapeutic response prediction with the formulated nomogram was 0.828 (95% CI 0.710–0.913).

Performance of the combined model

Diagnostic characteristics of significant features and their combination for predicting therapeutic responses are demonstrated in Table 4. When the significant MRI features above were combined, a largest AUC of 0.828 was achieved, superior to features of tumor margin ($z = 2.454$, $p = 0.0141$), T2WI

Table 3 Qualitative MRI characteristics of intrahepatic cholangiocarcinoma according to therapeutic response

Variables	Response (<i>n</i> = 30)	No response (<i>n</i> = 31)	<i>p</i>	ICC (95% CI)
Tumor number 1/2–5/> 5	20 (66.7)/5 (16.7)/5 (16.7)	9 (29.0)/4 (12.9)/18 (58.1)	0.003*	0.950 (0.919–0.970)
Location right/left/right and left/caudate lobe	12 (40.0)/8 (26.7)/10 (33.3)/0 (0)	12 (38.7)/13 (41.9)/5 (16.1)/1 (3.2)	0.250	0.951 (0.919–0.970)
Tumor margin smooth/irregular	22 (73.3)/8 (26.7)	11 (35.5)/20 (64.5)	0.005*	0.838 (0.743–0.899)
T2 homogeneity homogeneous/heterogeneous	11 (36.7)/19 (63.3)	1 (3.2)/30 (96.8)	0.001*	0.796 (0.682–0.872)
Arterial enhancement non-rim/rim/no enhancement	7 (23.3)/21 (70.0)/2 (6.7)	6 (19.4)/25 (80.6)/0 (0)	0.421	0.924 (0.876–0.954)
Arterial enhancement intensity marked/moderate/mild	1 (3.3)/25 (83.3)/4 (13.3)	3 (9.7)/27 (87.1)/1 (3.2)	0.267	0.702 (0.547–0.810)
Enhancement pattern progressive/persistent/washout	27 (90.0)/2 (6.7)/1 (3.3)	27 (87.1)/3 (9.7)/1 (3.2)	1.000	0.883 (0.812–0.929)
Arterial peritumoral enhancement Y/N	17 (56.7)/13 (43.3)	28 (90.3)/3 (9.7)	0.003*	0.866 (0.787–0.918)
Signal in DWI non-rim hyper-/rim hyperintensity	20 (66.7)/10 (33.3)	25 (80.6)/6 (19.4)	0.255	0.959 (0.933–0.975)
Targetoid appearance Y/N	21 (70.0)/9 (30.0)	25 (80.6)/6 (19.4)	0.384	0.850 (0.773–0.902)
Hemorrhage in mass Y/N	3 (10.0)/27 (90.0)	6 (19.4)/25 (80.6)	0.473	0.816 (0.711–0.886)
Necrosis in mass Y/N	17 (56.7)/13 (43.3)	23 (74.2)/8 (25.8)	0.184	0.965 (0.942–0.979)
Hepatic capsule retraction Y/N	12 (40.0)/18 (60.0)	18 (58.1)/13 (41.9)	0.204	0.935 (0.895–0.961)
Intrahepatic bile duct dilation Y/N	20 (66.7)/10 (33.3)	22 (71.0)/9 (29.0)	0.786	0.963 (0.929–0.978)

Unless otherwise specified, data are numbers of patients/lesions, with percentage in parentheses

Variables are analyzed using Pearson's χ^2 test or Fisher's exact test as appropriate

DWI diffusion-weighted imaging, ICC interclass correlation coefficient, CI confidence interval

* $p < 0.05$

homogeneity ($z = 3.402$, $p = 0.0007$), and APE ($z = 3.332$, $p = 0.0009$) alone.

Based on the receiving operating characteristic curve analysis, threshold value of the combined index was set as 0.47962. The 6-month and 12-month PFS rates for ICCs with high combined index values (> 0.47962) were 94.7% (95% CI 84.7–100.0%) and 78.9% (95% CI 60.5–97.3%), and PFS

rates for patients with low values (≤ 0.47962) were 71.4% (95% CI 57.7–85.1%) and 37.4% (95% CI 21.5–53.3%), respectively. ICCs with high combined index tended to take longer to progress than those with low values ($\chi^2 = 13.306$, $p < 0.0001$) (Fig. 5). Cox analysis showed that the combined index was independently associated with PFS (hazard ratio = 5.670 (95% CI 1.992, 16.136), $p = 0.001$), while the

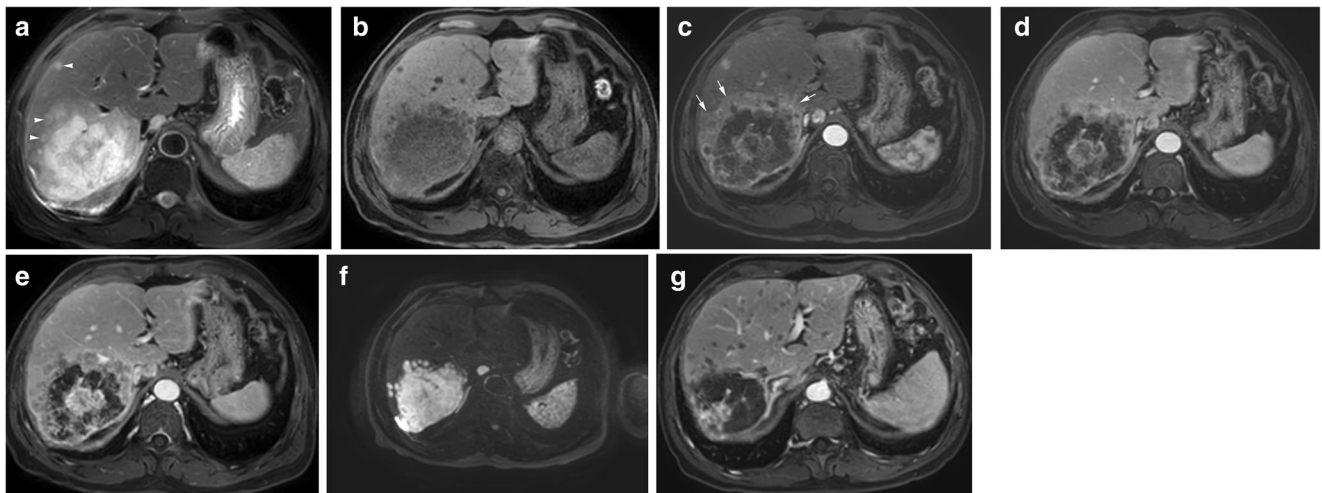


Fig. 2 Intrahepatic cholangiocarcinoma in a 67-year-old man. **a** T2-weighted image shows a large heterogeneous hyperintense tumor in the right lobe with irregular, ill-defined margin. Peripheral and distant intrahepatic satellite nodules are presented (white arrowheads). **b** Pre-contrast T1-weighted image shows a hypointense tumor. **c** Contrast-enhanced arterial phase image shows moderate rim enhancement accompanying

arterial peritumoral enhancement (white arrows). Contrast-enhanced portal venous (**d**) and delay phase (**e**) images show a progressive enhancement pattern. **f** Diffusion-weighted image exhibits non-rim hyperintensity. **g** Progression occurred at the first follow-up 2 months after the therapy with multiple new foci in the liver

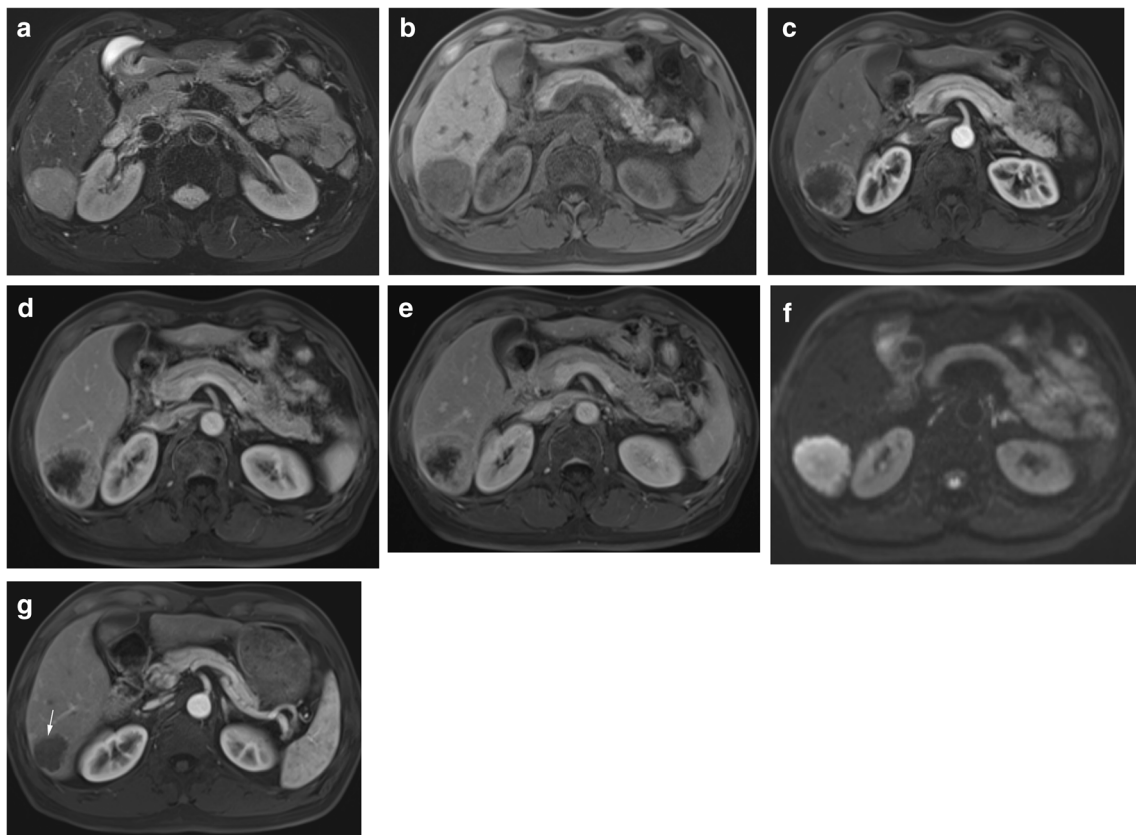


Fig. 3 Intrahepatic cholangiocarcinoma in a 66-year-old man. **a** T2-weighted image shows a homogeneous hyperintense tumor in the right lobe with smooth, well-defined margin. **b** Pre-contrast T1-weighted image shows a hypointense tumor. **c** Contrast-enhanced arterial phase image shows moderate rim enhancement without arterial peritumoral

enhancement. Contrast-enhanced portal venous (**d**) and delay phase (**e**) images show a progressive enhancement pattern. **f** Diffusion-weighted image exhibits non-rim hyperintensity. **g** Partial response with > 30% decrease in tumor diameter accompanying significant necrosis was observed at the first follow-up 2 months after therapy (white arrow)

therapeutic group was not a significant independent predictor ($p = 0.803$); and PFS rates were not different between the three treatment groups ($\chi^2 = 1.369$, $p = 0.504$).

Discussion

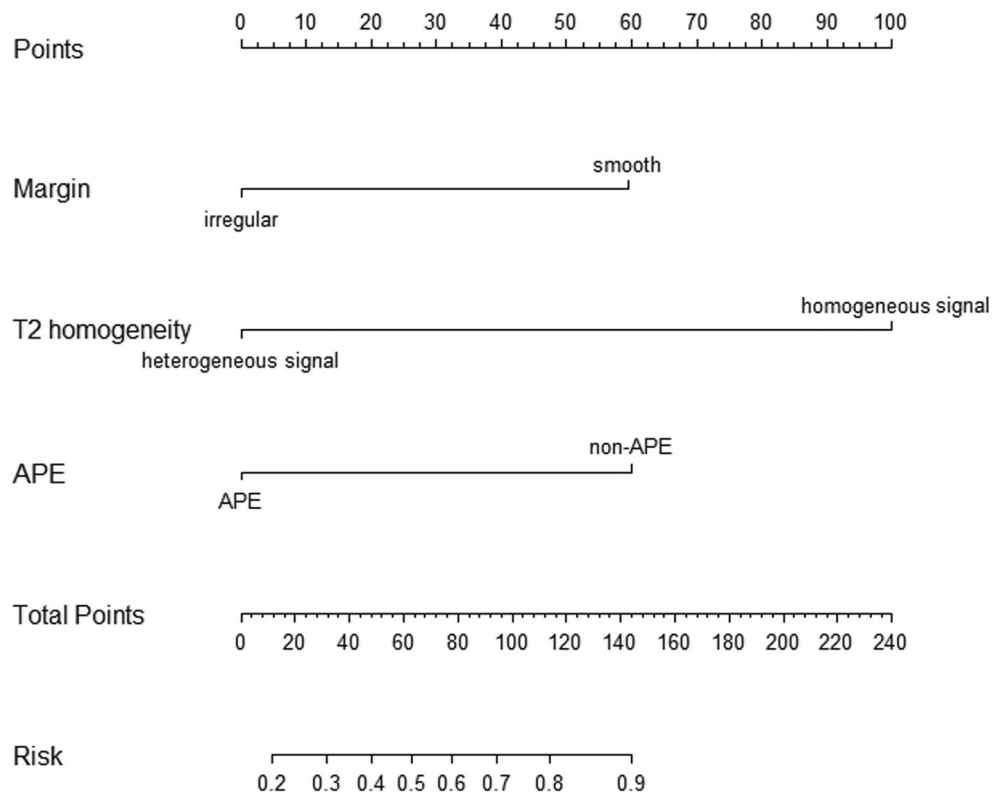
ICC is an aggressive primary liver cancer of the biliary duct system with extremely poor therapeutic outcomes [17]. Advanced-stage ICC remains a difficult-to-treat disease to date; the combined systemic strategies may be a promising therapeutic direction. However, differential responses to treatment have been observed attributing to the inherent heterogeneity of tumor and immune microenvironment of different individual patients. Timely and accurate assessment of tumor response to therapy is needed to select suitable candidates, for both therapeutic and prognostic purposes. In this study, we confirmed the feasibility of the combined systemic treatment with targeted therapy, immunotherapy, and/or chemotherapy with an overall response rate of 49.18%. Moreover, the results of this study demonstrated that MRI features of smooth margin, homogeneous T2 signal, and non-APE were potential

predictors of therapeutic response in advanced ICC, and the combination model incorporating the three significant MRI features manifested an improved predictive value with high specificity.

Irregular tumor margin was related to negative therapeutic response of ICC in our study. Tumors with irregular margin are rich in pathological vessels around and may be related to tumor aggressiveness [18]. These tumors usually show an infiltrative growth pattern and tend to invade small portal venous vessels around the tumor, which may result in the formation of satellite nodules; the fusion of the primary mass and adjacent satellite nodules may result in an ill-defined shape [19].

Our study showed that T2 homogeneity was a predictor for therapeutic response, and heterogeneous signal was more commonly seen in non-response ICCs. Heterogeneous signal may indicate the presence of complex intratumoral components, referring to tumor heterogeneity with histological variations and potential rapid growth [20]. Moreover, inherent tumor heterogeneity might hamper disease remission and palliation as well as promote the metastatic behavior, and further lead to drug resistance and treatment failure [21, 22]. Thus,

Fig. 4 Nomogram for therapeutic response prediction. The nomogram established by combining tumor margin, T2 homogeneity, and arterial peritumoral enhancement (APE). Predictor points are on uppermost point scale corresponding to each variable. On the bottom scale, points for all variables are added and translated into response probability



there are good reasons to believe that T2 homogeneity might convey prognostic information and play a role in patient selection for systemic therapy.

We also identified the role of the imaging feature of APE in the prediction of therapeutic response. APE presents abnormal hemodynamic perfusions surrounding the tumor due to portal branch microthrombosis and compensatory increased arterial blood supply [23, 24]. Researches have proven that APE is a predictive biomarker for microvascular invasion in both hepatocellular carcinoma [24–26] and combined hepatocellular-cholangiocarcinoma [23, 27], which is closely related to worse clinical outcomes. Our study indicated its potential predictive value in ICC.

The combined index incorporating the significant imaging features above achieved a best predictive performance with

high specificity, and the MRI-based nomogram showed satisfactory predictive performance across the spectrum of response prediction (C-index: 0.828) which refined the accuracy of estimation. In the meantime, our results proved that the MRI-based combined index can be regarded as a reliable and independent predictor of response, taking the potential confounding factor of different therapies into account. Thus, contrast-enhanced MRI may serve as a practical non-invasive tool to select more targeted candidates in real-world practice. If adverse outcome is predicted by MRI assessment, unnecessary therapies could be avoided for those potential poorly responding patients. However, the sensitivity of the combination model has yet to be improved, and our results needed to be verified by future multicenter studies with external validation to improve generalization. Moreover, our results verified

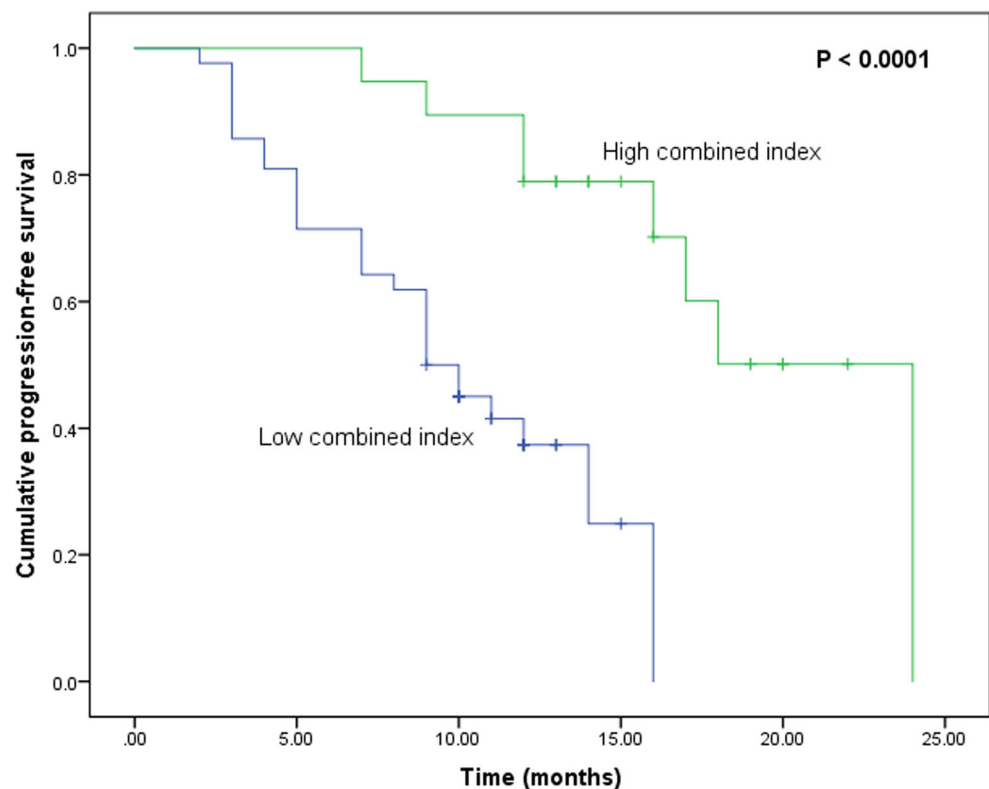
Table 4 Diagnostic performance of significant findings and their combination for therapeutic response prediction of intrahepatic cholangiocarcinoma

	AUC	Sensitivity (%)	Specificity (%)	LR+ (%)	LR- (%)
Smooth margin	0.689 (0.558–0.802)	73.33 (54.1–87.7)	64.52 (45.4–80.8)	2.07 (1.2–3.5)	0.41 (0.2–0.8)
Homogeneous T2 signal	0.667 (0.535–0.783)	36.67 (19.9–56.1)	96.77 (83.3–99.9)	11.37 (1.6–82.7)	0.65 (0.5–0.9)
No APE	0.668 (0.536–0.784)	43.33 (25.5–62.6)	90.32 (74.2–98.0)	4.48 (1.4–14.2)	0.63 (0.4–0.9)
Combined index	0.828 (0.710–0.913)	56.67 (37.4–74.5)	93.55 (78.6–99.2)	8.78 (2.2–34.8)	0.46 (0.3–0.7)

Data in parentheses are 95% confidence intervals

AUC area under the curve, LR likelihood ratio, APE arterial peritumoral enhancement

Fig. 5 Progression-free survival of intrahepatic cholangiocarcinomas with high combined index and low combined index. Patients with high combined index values showed higher cumulative progression-free survival rates than those with low values ($p < 0.0001$). Threshold value of the combined index was set as 0.47962 based on the corresponding receiving operating characteristic curve analysis



that ICCs with high combined index values tended to take longer to progress than those with low values, confirming its worth in pre-treatment response evaluation.

In addition, the results of univariate analysis showed that increasing lesion number impaired therapeutic efficacy as well, although it was not an independent factor. An increase in the number of tumors indicated higher tumor burden within a more advanced tumor stage, which represented an essential prognostic factor for poor survival of ICC [28].

Our study had several limitations. First, the sample size was relatively small; thus, our preliminary results should be verified with larger study population. Second, as one of the clinical trials was carried on since February 2020, and the last patient participated in September 2020, long-term survival data was not included in the present study. Future study with sufficient follow-up data needs to be further fulfilled. Third, the retrospective nature leads to inherent bias, including patient selection. Additionally, we only included advanced ICC patients who received first-line systemic therapy; our results need to be validated in patients with second- or third-line systemic therapy, or patients who undergo conversion resection with pathologic response results. Finally, the datasets of two clinical trials with different therapeutic regimens were pooled in our study. According to our results, although different therapies were not equally distributed over different response groups, the therapeutic group was not an independent confounding factor. Thus, we considered it reasonable to include both groups in a single analysis. Moreover, by pooling different therapies, it could be a

promising non-invasive assessment to test in a broader population. And yet, subgroup analysis of respective therapy protocols is valuable in future work.

According to our preliminary research, MRI features including tumor margin, T2 homogeneity, and APE were potential predictors of therapeutic response in advanced ICC with systemic therapy, and the combination model incorporating the three significant MRI features achieved an improved predictive value, which may play an important role in identifying appropriate therapeutic candidates and optimize individual treatment strategies.

Acknowledgements This study was funded by the Natural Science Foundation of Fujian Province (grant number 2021D032), Shanghai Rising Stars of Medical Talent Youth Development Program (grant number SHWRS(2020)_087), the Shanghai Municipal Key Clinical Specialty (grant number shslczdzk03202), and the Clinical Research Plan of SHDC (grant number SHDC2020CR1003A). The authors thank the statistician Minzhi Lv for her support in statistical analyses in this work.

Funding This study has received funding by the Natural Science Foundation of Fujian Province (grant number 2021D032), Shanghai Rising Stars of Medical Talent Youth Development Program (grant number SHWRS(2020)_087), the Shanghai Municipal Key Clinical Specialty (grant number shslczdzk03202), and the Clinical Research Plan of SHDC (grant number SHDC2020CR1003A).

Declarations

Guarantor The scientific guarantor of this publication is Mengsu Zeng.

Conflict of interest The authors of this manuscript declare no relationships with any companies whose products or services may be related to the subject matter of the article.

Statistics and biometry One of the authors has significant statistical expertise (Shanshan Gao). And Minzhi Lv kindly provided statistical advice for this manuscript.

Informed consent Written informed consent was waived by the Institutional Review Board.

Ethical approval Institutional Review Board approval was obtained by Zhongshan Hospital, Fudan University (Approval Number: B2021-113R).

Methodology

- retrospective
- diagnostic or prognostic study
- performed at one institution

References

1. Sirica AE, Gores GJ, Groopman JD et al (2019) Intrahepatic cholangiocarcinoma: continuing challenges and translational advances. *Hepatology* 69:1803–1815
2. Kelley RK, Bridgewater J, Gores GJ, Zhu AX (2020) Systemic therapies for intrahepatic cholangiocarcinoma. *J Hepatol* 72:353–363
3. Fiteni F, Nguyen T, Vernerey D et al (2014) Cisplatin/gemcitabine or oxaliplatin/gemcitabine in the treatment of advanced biliary tract cancer: a systematic review. *Cancer Med* 3:1502–1511
4. Jang JS, Lim HY, Hwang IG et al (2010) Gemcitabine and oxaliplatin in patients with unresectable biliary cancer including gall bladder cancer: a Korean Cancer Study Group phase II trial. *Cancer Chemother Pharmacol* 65:641–647
5. Llovet JM, Ricci S, Mazzaferro V et al (2008) Sorafenib in advanced hepatocellular carcinoma. *N Engl J Med* 359:378–390
6. Kudo M, Finn RS, Qin S et al (2018) Lenvatinib versus sorafenib in first-line treatment of patients with unresectable hepatocellular carcinoma: a randomised phase 3 non-inferiority trial. *Lancet* 391:1163–1173
7. Ueno M, Ikeda M, Sasaki T et al (2020) Phase 2 study of lenvatinib monotherapy as second-line treatment in unresectable biliary tract cancer: primary analysis results. *BMC Cancer* 20:1105
8. El-Khoueiry AB, Sangro B, Yau T et al (2017) Nivolumab in patients with advanced hepatocellular carcinoma (CheckMate 040): an open-label, non-comparative, phase 1/2 dose escalation and expansion trial. *Lancet* 389:2492–2502
9. Finn RS, Ryoo BY, Merle P et al (2020) Pembrolizumab as second-line therapy in patients with advanced hepatocellular carcinoma in KEYNOTE-240: a randomized, double-blind, phase III trial. *J Clin Oncol* 38:193–202
10. Ilyas FZ, Beane JD, Pawlik TM (2021) The state of immunotherapy in hepatobiliary cancers. *Cells* 10:2096
11. Lee YJ, Lee JM, Lee JS et al (2015) Hepatocellular carcinoma: diagnostic performance of multidetector CT and MR imaging—a systematic review and meta-analysis. *Radiology* 275:97–109
12. Kudo M (2020) Gd-EOB-DTPA-MRI could predict WNT/beta-catenin mutation and resistance to immune checkpoint inhibitor therapy in hepatocellular carcinoma. *Liver Cancer* 9:479–490
13. Yoon JH, Lee JM (2019) Can MRI features predict prognosis in mass-forming intrahepatic cholangiocarcinoma? *Radiology* 290:700–701
14. Pandey A, Pandey P, Ghasabeh MA et al (2018) Baseline volumetric multiparametric MRI: can it be used to predict survival in patients with unresectable intrahepatic cholangiocarcinoma undergoing transcatheter arterial chemoembolization? *Radiology* 289:843–853
15. Kim S, An C, Han K, Kim MJ (2019) Gadoteric acid enhanced magnetic resonance imaging for prediction of the postoperative prognosis of intrahepatic mass-forming cholangiocarcinoma. *Abdom Radiol (NY)* 44:110–121
16. Eisenhauer EA, Therasse P, Bogaerts J et al (2009) New response evaluation criteria in solid tumours: revised RECIST guideline (version 1.1). *Eur J Cancer* 45:228–247
17. Bertuccio P, Malvezzi M, Carioli G et al (2019) Global trends in mortality from intrahepatic and extrahepatic cholangiocarcinoma. *J Hepatol* 71:104–114
18. Chen J, Wu Z, Xia C et al (2020) Noninvasive prediction of HCC with progenitor phenotype based on gadoteric acid-enhanced MRI. *Eur Radiol* 30:1232–1242
19. Zhao YJ, Chen WX, Wu DS, Zhang WY, Zheng LR (2016) Differentiation of mass-forming intrahepatic cholangiocarcinoma from poorly differentiated hepatocellular carcinoma: based on the multivariate analysis of contrast-enhanced computed tomography findings. *Abdom Radiol (NY)* 41:978–989
20. Wei Y, Pei W, Qin Y, Su D, Liao H (2021) Preoperative MR imaging for predicting early recurrence of solitary hepatocellular carcinoma without microvascular invasion. *Eur J Radiol* 138:109663
21. Ahn KS, Kang KJ (2020) Molecular heterogeneity in intrahepatic cholangiocarcinoma. *World J Hepatol* 12:1148–1157
22. Braconi C, Roessler S, Kruk B, Lammert F, Krawczyk M, Andersen JB (2019) Molecular perturbations in cholangiocarcinoma: is it time for precision medicine? *Liver Int* 39(Suppl 1):32–42
23. Wang X, Wang W, Ma X et al (2020) Combined hepatocellular-cholangiocarcinoma: which preoperative clinical data and conventional MRI characteristics have value for the prediction of microvascular invasion and clinical significance? *Eur Radiol* 30:5337–5347
24. Chong HH, Yang L, Sheng RF et al (2021) Multi-scale and multiparametric radiomics of gadoterate disodium-enhanced MRI predicts microvascular invasion and outcome in patients with solitary hepatocellular carcinoma ≤ 5 cm. *Eur Radiol* 31:4824–4838
25. Zhao H, Hua Y, Dai T et al (2017) Development and validation of a novel predictive scoring model for microvascular invasion in patients with hepatocellular carcinoma. *Eur J Radiol* 88:32–40
26. Yang L, Gu D, Wei J et al (2019) A radiomics nomogram for preoperative prediction of microvascular invasion in hepatocellular carcinoma. *Liver Cancer* 8:373–386
27. Zhou C, Wang Y, Ma L, Qian X, Yang C, Zeng M (2021) Combined hepatocellular carcinoma-cholangiocarcinoma: MRI features correlated with tumor biomarkers and prognosis. *Eur Radiol* 32:78–88
28. King MJ, Hectors S, Lee KM et al (2020) Outcomes assessment in intrahepatic cholangiocarcinoma using qualitative and quantitative imaging features. *Cancer Imaging* 20:43

Publisher's note Springer Nature remains neutral with regard to jurisdictional claims in published maps and institutional affiliations.